



Automated nailfold capillary density measurement method based on improved YOLOv5



Hao Yin ^{a,1}, Zhiwei Wu ^{a,1}, An Huang ^b, Jiaxiong Luo ^a, Junzhao Liang ^a, Jianan Lin ^a, Qianyao Ye ^a, Mugui Xie ^a, Cong Ye ^a, Xiaosong Li ^a, Yanxiong Wu ^{a,c,*}

^a School of Physics and Optoelectronic Engineering, Foshan University, Foshan 528000, China

^b School of Mechatronic Engineering and Automation, Foshan University, Foshan 528000, China

^c Ji Hua Laboratory, Foshan, Guangdong 528200, China

ARTICLE INFO

Keywords:

Nailfold capillary density
Automatic measurement
YOLOv5
Deep learning
90° method

ABSTRACT

Nailfold capillary density is an essential physiological parameter for analyzing nailfold health; however, clinical images of the nailfold are taken in many situations, and most clinicians subjectively analyze nailfold images. Therefore, based on the improved “you only look once v5” (YOLOv5) algorithm, this study proposes an automated method for measuring nailfold capillary density. The improved technique can effectively and rapidly detect distal capillaries by incorporating methods or structures such as 9mosaic, spatial pyramid pooling cross-stage partial construction, bilinear interpolation, and efficient intersection over union. First, the modified YOLOv5 algorithm was used to detect nailfold capillaries. Subsequently, the number of distal capillaries was filtered using the 90° method. Finally, the capillary density was calculated. The results showed that the Average Precision (AP)@0.5 value of the proposed approach reached 85.2 %, which was an improvement of 4.93 %, 5.24 %, and 107 % compared with the original YOLOv5, YOLOv6, and simple-faster rapid-region convolutional network (R-CNN), respectively. For different nailfold images, using the density calculated by nailfold experts as a benchmark, the calculated results of the proposed method were consistent with the manually calculated results and superior to those of the original YOLOv5.

1. Introduction

Microcirculation comprises 99 % of adult blood vessels (Neubauer-Geryk et al., 2019) and is regulated between the arteries and veins of the cardiovascular system. Its primary function is to exchange nutrients and waste products between the blood and tissues. Pathological changes in the microcirculation reflect changes in the body during ailments. Therefore, studying microcirculation aids diagnosis (Tian et al., 2020). The common microcirculatory locations in the body include the nailfold, retina (Sallialmi et al., 2012), and sublingual surface (Emrani et al., 2017). Nailfold microcirculation is an essential area of clinical microcirculation research because it can be compromised in systemic diseases or specific skin conditions. Therefore, studying it can prevent certain diseases or detect and treat them early (Hofstee et al., 2012).

A significant physiological parameter for detecting nailfold microcirculation is the nailfold capillary density, defined as the number of distal capillaries per millimeter span of each finger or toe (Hofstee et al.,

2012; Ong et al., 1998). In studies of conditions such as connective tissue disease, chronic kidney disease, pulmonary hypertension in patients with scleroderma (Maldonado et al., 2022), and diabetes (Karbalaei et al., 2017), nailfold capillary density was a crucial quantitative parameter.

The nailfold capillary density used to be measured manually by physicians; however, the clinical measurement of this parameter is subjective and can be ambiguous (Lambova et al., 2011), affecting diagnosis. Hence, developing a fully automated process for measuring nailfold capillary density is essential. In most previous studies, the direct observation method (DO) (Gracia Tello et al., 2022) was used to measure capillary density. However, the method is time-consuming, and a lengthy analysis increases the subjectivity of the results. Thus, Hosftee et al. proposed the 90° method to replace the DO method, significantly improving the accuracy (Hofstee et al., 2012); however, the time-consuming challenge persisted, preventing real-time detection. Furthermore, Karbalaei et al. proposed the elliptical broken line method

* Corresponding author at: School of Physics and Optoelectronic Engineering, Foshan University, Foshan 528000, China.

E-mail address: wuyanxiong@fosu.edu.cn (Y. Wu).

¹ Hao Yin and Zhiwei Wu contributed equally to this work.

(Karbalaie et al., 2017), based on the 90° method, and developed a Graphical User Interface (GUI) program for semi-automatic detection of capillaries; however, clinically achieving real-time detection remained impossible and required manual marking of vessels. In a recent study, Tello et al. developed a deep learning system for the fully automated measurement of nailfold capillary parameters (Gracia Tello et al., 2022), which can measure most nailfold vessel parameters. The accuracy of this system is comparable to that of the algorithm used in this study regarding vessel density measurement. However, the field of view is small and does not consider the various conditions in the captured nailfold images. These methods provide a theoretical basis for the automatic detection of nailfold capillaries.

With the increasing deep learning target detection algorithms, the algorithms have evolved into two-stage network models, such as the rapid region convolutional network (R-CNN) (Girshick and Fast, 2015), Faster R-CNN (Ren et al., 2017) and one-stage network models, such as YOLO (Redmon et al., 2016). Among them, the YOLO algorithm dominates with its excellent performance and simple deployment. Researchers apply this algorithm to other fields. Lawal proposed an improved YOLOv3 model called YOLO-Tomato (Lawal, 2021) and developed three versions of the model: a, b, and c, with Average Precision (AP) values exceeding 98 %. Similarly, Cao et al. proposed a GhostNet-YOLOv5 algorithm for detecting tea buds based on the YOLOv5 algorithm (Cao et al., 2022). The GhostNet-YOLOv5 algorithm reduced the model size and improved the program speed, achieving an accuracy of 76.31 %, improving the accuracy of tea bud detection. Moreover, Tian et al. proposed a high-precision detection method for aerial remote sensing image target detection, KCFS-YOLOv5 (Tian et al., 2023), using the K-means++ method to optimize the primary cluster points, and introduced a bidirectional feature pyramid network to improve the detection accuracy of small targets. This study showed that the method is significantly accurate in aerial remote-sensing images. The above processes provide a theoretical basis for combining the YOLOv5 algorithm and measurement of nailfold capillary density.

Given the excellent performance of the YOLO algorithm in many specialized fields and the clinical need for real-time detection, we used YOLOv5 as a framework. We improved it by combining the nailfold capillary characteristics to achieve accurate nailfold capillary density measurements. First, the 4mosaic data enhancement method in the input layer was replaced by a 9mosaic method to improve the robustness of the algorithm. Second, spatial pyramid pooling (SPP) (He et al., 2015) was replaced by spatial pyramid pooling cross-stage partial convolution (SPPCSPC), and the upsampling method (improving feature map resolution) was changed to bilinear interpolation to improve the feature extraction and feature fusion capabilities of the network. Finally, an efficient intersection over union (EIOU) (Zhang et al., 2022) was used as a location loss to improve the backpropagation and detection

performance.

2. Materials and methods

2.1. Research devices

The experimental setup used in this study is shown in Fig. 1. Experimental equipment A (Fig. 1-A) comprised primarily a CMOS camera (Mshot-MSX11 microscope), an optical system, an LED light source, and a finger holder. The image resolution is 5280 × 3956 pixels with a pixel size of 3.3 × 3.3 μm and 17.42 mm × 13.05 mm field of view. The optical system had an objective lens with a numerical aperture of 0.3 and a magnification of 5.5 X. The custom LED light source had a power of 3 W and a color temperature of 10,000 K. Part of the data acquisition was based on experimental equipment B (CMOS camera for the Mshot-MDX10 microscope with a resolution of 5480 × 3648 pixels, a pixel size of 2.4 × 2.4 μm, and a magnification of 5.5 X) (Fig. 1-B).

2.2. Research participants

Thirty healthy volunteers were selected for nailfold capillary imaging. They were placed in a room at 22–24 °C for 10–20 min before imaging. Subsequently, the participants were asked to wash their hands after 20 min and allow them to dry naturally before placing a drop of cedar oil on the nailfold to improve light transmission (El Miedany et al., 2022). Throughout the imaging process, the participants were asked to sit upright and keep their heart position flush with their hands (Silva et al., 2016). A sample nailfold image is shown in Fig. 2.

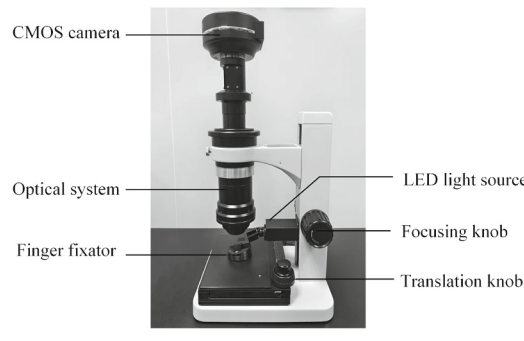
3. Method

3.1. Improved YOLOv5 algorithm

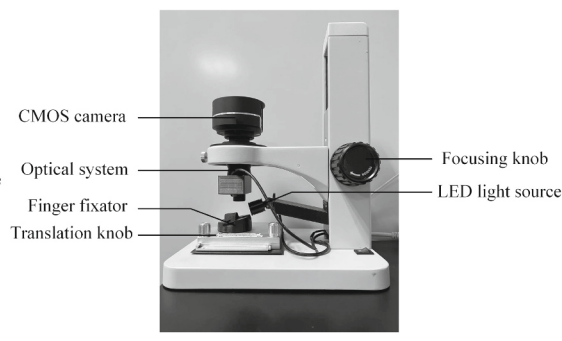
YOLO is a target detection algorithm based on a convolutional neural network. This is a pioneering one-step detection. One-step algorithms can directly generate an object's class probability and position coordinate values, and the final detection result can be obtained after a single detection. Therefore, YOLO can be used for end-to-end detection (Redmon and Farhadi, 2017). YOLO has been updated since its release in 2016 and has undergone several iterations from version 1 to version 5 in five years (Asad et al., 2022). In this study, we combined the previous changes and made relevant improvements to the YOLOv5 algorithm based on the morphological properties of nailfold capillaries. The improved network model is shown in Fig. 3.

The improvements are as follows:

Input: The 4mosaic method was replaced with the 9mosaic method. This is a general technique that improves the sample quality at the input



Experimental equipment Figure
A



Experimental equipment Figure
B

Fig. 1. Experimental equipment for taking nailfold images.



Fig. 2. Sample nailfold image.

end, which can significantly enhance the robustness of the algorithm. The flow of the mosaic method is shown in Fig. 4. The primary idea of the mosaic method was to randomly crop, scale, arrange, and stitch images to form a single image to achieve a richer dataset while improving the training speed of the network. The 4mosaic method involves using four images, and the 9mosaic method is conducted with nine. Compared with the 4mosaic method, the 9mosaic method further improves the dataset's quality and increases the model's generalizability.

Backbone network: Because most healthy capillaries are upside-down U-shaped or hairpin-shaped, the shape is unique but uniform; therefore, when performing blood vessel detection, our proposed method should be more sensitive to the shape of the object. Although SPPCSPC involves slightly more calculation, it can greatly improve the method's ability to extract object shape information. The SPP structure (Fig. 5) was replaced with the SPPCSPC structure (Fig. 6). The SPP structure is used to perform a max pooling operation (dividing the input feature map into several rectangular areas, with output of the maximum value for each sub-area) on the feature maps through three convolutional kernels of different sizes followed by a concat operation (splicing two feature maps in the channel dimension) on these three pooled feature maps to achieve an adaptive size output. The SPPCSPC structure is first used to conduct regular processing of the feature map, while a copy of the input feature map is processed in the SPP structure, and the two parts are merged. Compared with the SPP structure, it further improves the model's ability to extract and fuse object features and the detection performance of the algorithm.

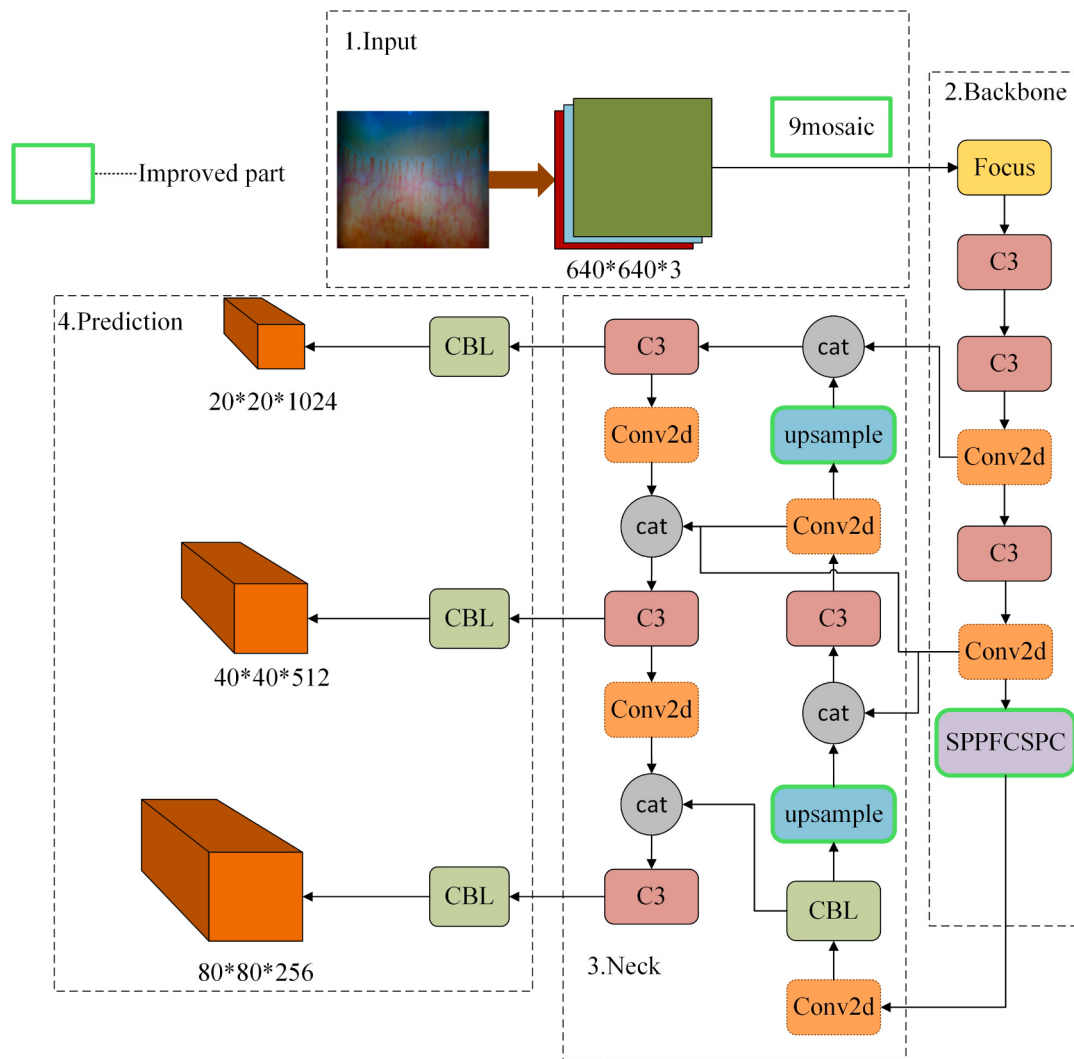
Neck network: When detecting nailfold capillaries, there may be dense, tiny blood vessels in some areas. In this case, information is easily

lost during the upsampling process. Therefore, upsampling is changed from nearest-neighbor interpolation to bilinear interpolation. Nearest-neighbor interpolation, also known as zero-order interpolation, is a more straightforward form of upsampling in which the grey value of a transformed pixel is equal to that of the nearest input pixel. In contrast, bilinear interpolation is used to calculate the weighted average of the properties (color and opacity, among others) of the four surrounding texture pixels and apply it to the screen pixel. Compared with nearest-neighbor interpolation, bilinear interpolation significantly preserves the accuracy of the image pixels during upsampling.

Output: Owing to the small size of nailfold capillaries compared to that of the entire image, more accurate position information must be propagated when the algorithm is backpropagating; therefore, the loss function was used by replacing complete intersection over union (CIOU) with EIOU. The CIOU loss considers the overlap area, centroid distance, and aspect ratio of the bounding box regression. The CIOU is defined as

$$l_{CIOU} = 1 - \left(IOU - \frac{(Distance_2)^2}{(Distance_C)^2} \right) + \alpha v \quad (1)$$

In Formula (1), the Intersection Over Union (IOU) denotes the intersection ratio of the real box (manually labeled), and the predicted box, C denotes the smallest outer rectangle of the two boxes, $Distance_C$ denotes the diagonal distance between the smallest external rectangles of the two frames, $Distance_2$ denotes the Euclidean distance between the center points of the two frames, v is a parameter for measuring the consistency of the aspect ratio, and α is a balancing factor for measuring the losses caused by the aspect ratio against the losses caused by the IOU component. α and v are defined as



CBL:Abbreviation for Conv+BN(BatchNormalization)+Leaky RELU(Rectified Linear Unit)
 RELU:Rectified Linear Unit
 cat:Abbreviation for concat

Fig. 3. Improved YOLOv5 network structure (the green boxes are the improvements in this study).

$$\alpha = \begin{cases} 0 & \text{if } IOU < 0.5 \\ \frac{v}{(1 - IOU) + v} & \text{if } IOU \geq 0.5 \end{cases} \quad (2)$$

$$v = \frac{4}{\pi^2} \left(\arctan \frac{w^{gt}}{h^{gt}} - \arctan \frac{w^p}{h^p} \right)^2 \quad (3)$$

In Eq. (3), gt represents the ground truth boxes (manually labeled), and p represents the predicted boxes.

However, in CIOU, the aspect ratio is defined as a relative value rather than the true difference in width or height and its confidence level, which prevents the model from effectively optimizing similarity. The EIOU replaces the CIOU by splitting the aspect ratio effect factor based on the CIOU and calculating the length and width of the predicted and true boxes separately. EIOU is defined as:

$$l_{EIOU} = 1 - IOU + \frac{(Distance_2_h)^2}{(Distance_C)^2} + \frac{(Distance_2_w)^2}{(Distance_C_h)^2} + \frac{(Distance_2_w)^2}{(Distance_C_w)^2} \quad (4)$$

In Formula (4), $Distance_2_h$ and $Distance_2_w$ denote the Euclidean distance between the height and width of the two boxes. $Distance_C_h$ and

$Distance_C_w$ denote the height and width of the minimum enclosing rectangle of the two boxes, respectively.

Based on CIOU, EIOU replaces the aspect ratio with the difference in width and height, making the model converge faster and improving backpropagation ability.

3.2. Distal capillary filtering

To measure the density of nailfold capillaries, the YOLOv5 algorithm proposed in this study was used to detect nailfold images and filter the distal capillaries from the results. The 90° method is currently the mainstream technique for screening distal vessels. The principle is simple to understand and easy to implement in code; therefore, the 90° method was chosen for screening distal capillaries in this study. The principle of the 90° method, shown in Fig. 7, is that the apical midpoints of the target, adjacent left, and adjacent right vessels are the three points of a triangle. The angle between these three vessels is calculated using the Pythagorean rule. If the angle is <90°, it is not a distal capillary (Fig. 7-a); if it is >90°, it is a distal capillary (Fig. 7-b).

The screening process of our method was as follows: the nailfold

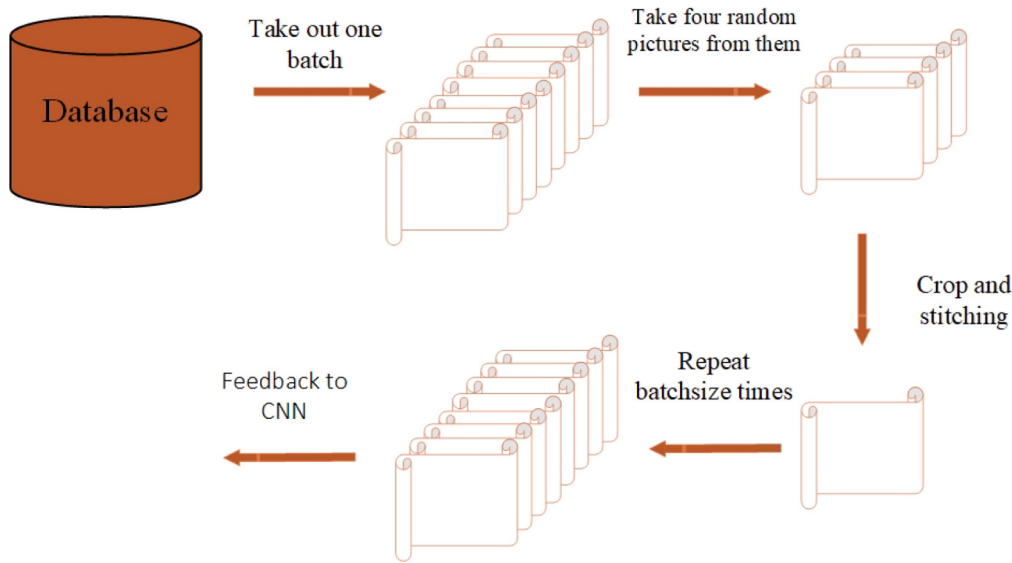
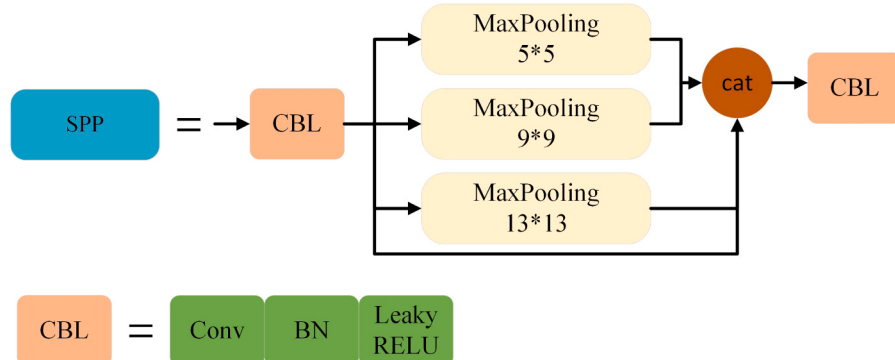


Fig. 4. Mosaic method process.



CBL:Abbreviation for Conv+BN(BatchNormalization)+Leaky RELU(Rectified Linear Unit)
 RELU:Rectified Linear Unit
 cat:Abbreviation for concat

Fig. 5. Spatial pyramid pooling structure.

image was first detected using the YOLOv5 algorithm proposed in this study, and the distal nailfold capillaries were screened out from the detected vessels using the 90° method, as shown in Fig. 8.

4. Results and discussion

4.1. Data sets

Thirty volunteers were selected to take 1788 nailfold images, requiring 10–20 s for acquisition of each image, and the images covered all nail areas. Five staff members spent approximately four hours allocating the 1788 images to one of four categories (representative images in Fig. 9): 1285 normal nailfold images, 9 images with stray light, 31 overexposed images, 300 images with many tiny blood vessels, and 163 unusable nailfold images due to poor focus or blur caused by motion artifact. This study selected 200 high-quality images (example in Fig. 2) from 1285 normal nailfold images for deep learning method training (the proposed method and the comparison method). Images with stray light, overexposure, and many tiny blood vessels were used for follow-up experiments. The nailfold images were annotated using the software, and the only category annotated was nailfold capillaries. Training,

testing, and validation were performed at a ratio of 6:2:2.

4.2. Experimental platform

This study was conducted using the PyTorch framework (version 1.12.1). The software and hardware configuration parameters are listed in Table 1.

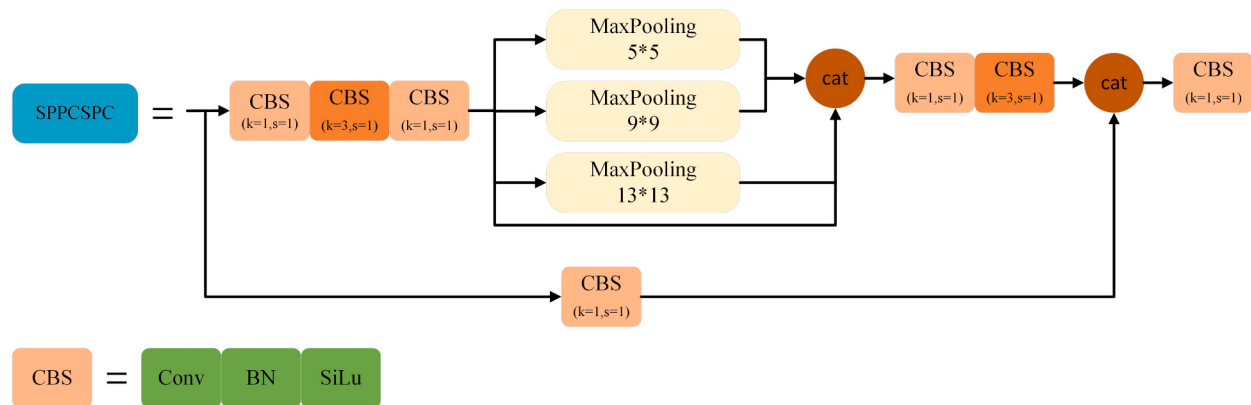
4.3. Evaluation indicators

This study focused on the precision, recall, and AP values of nailfold microvessel identification and used them as evaluation metrics. In addition, this experiment compared the algorithm performance from another aspect through the number of parameters, weight size, and average detection time.

Precision (P) is the proportion of positive samples in the identification sample

$$\text{precision} = \frac{t_p}{t_p + f_p} = \frac{t_p}{n} \quad (5)$$

Recall (R) is the proportion of all positive samples correctly



CBS:Abbreviation for Conv+BN(BatchNormalization)+SiLU(Sigmoid Linear Unit)
 SiLU:Sigmoid Linear Unit
 cat:Abbreviation for concat

Fig. 6. Spatial pyramid pooling cross-stage partial convolution structure.

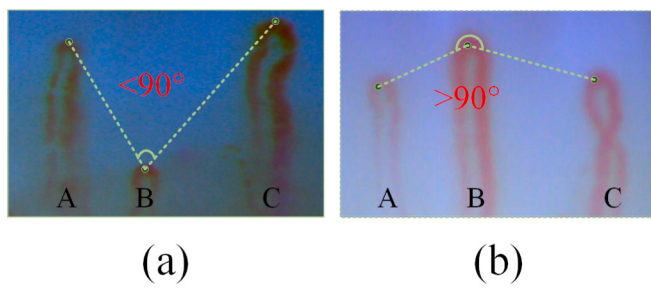


Fig. 7. 90° method of screening distal capillaries. The B capillary in (a) is not a distal capillary; the B capillary in (b) is a distal capillary.

identified as positive.

$$\text{Recall} = \frac{t_p}{t_p + f_n} \quad (6)$$

In Formulas (5) and (6), t_p refers to the actual positive and predicted positive results, f_p refers to the actual negative and predicted positive results, and f_n refers to the actual positive and predicted negative results.

The PR curve was plotted with recall on the abscissa and precision on the ordinate. The area under the PR curve is the AP score of the model. The AP value is an evaluation metric for mainstream deep learning models.

$$AP = \int_0^1 P(r)dr \quad (7)$$

In addition, 0.5 in AP@0.5 means that the confidence of IOU is 0.5. Commonly used confidence levels are 0.5, 0.75, or 0.5–0.95, and 0.5 was selected as the confidence level of IOU in this study.

Parameters refers to the total number of parameters that need to be trained in the network model. As the number of parameters increases, the time required to train the model increases. In this study, the summary method in the `pytorch_model_summary` library was used to directly calculate parameters.

Weight size refers to the physical size of the weight file obtained after model training. Weight size does not directly affect model inference performance. However, in one respect, the number of parameters will affect memory usage, and on the contrary, it will also affect the program initialization time.

The *detection time* refers to the time required for the model to detect a picture. *Average detection time* refers to the average time required for the

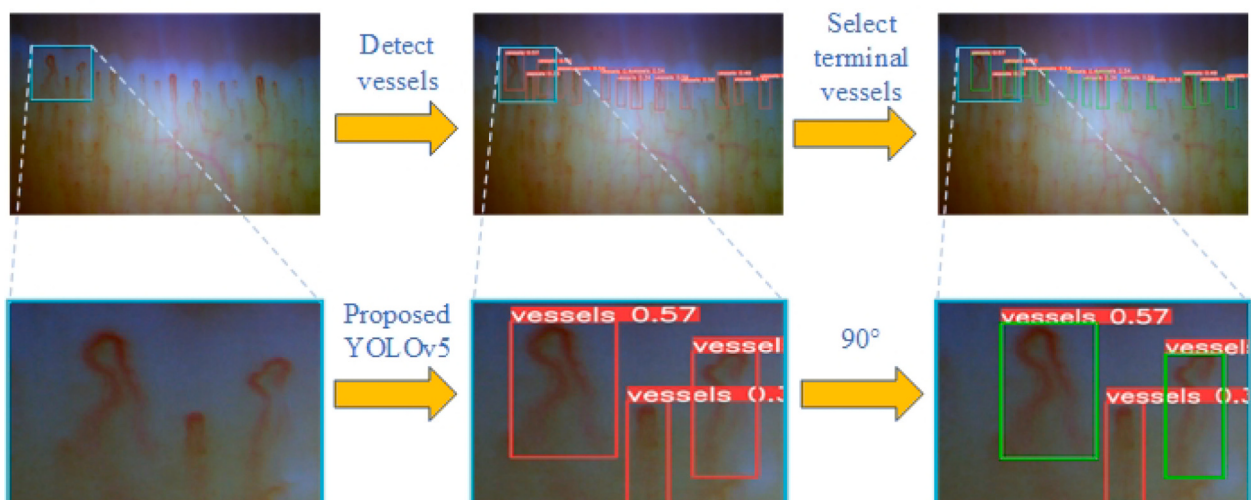


Fig. 8. Method proposed in this study screens distal capillaries (red boxes are YOLOv5 detect results, green boxes are screened distal capillaries).

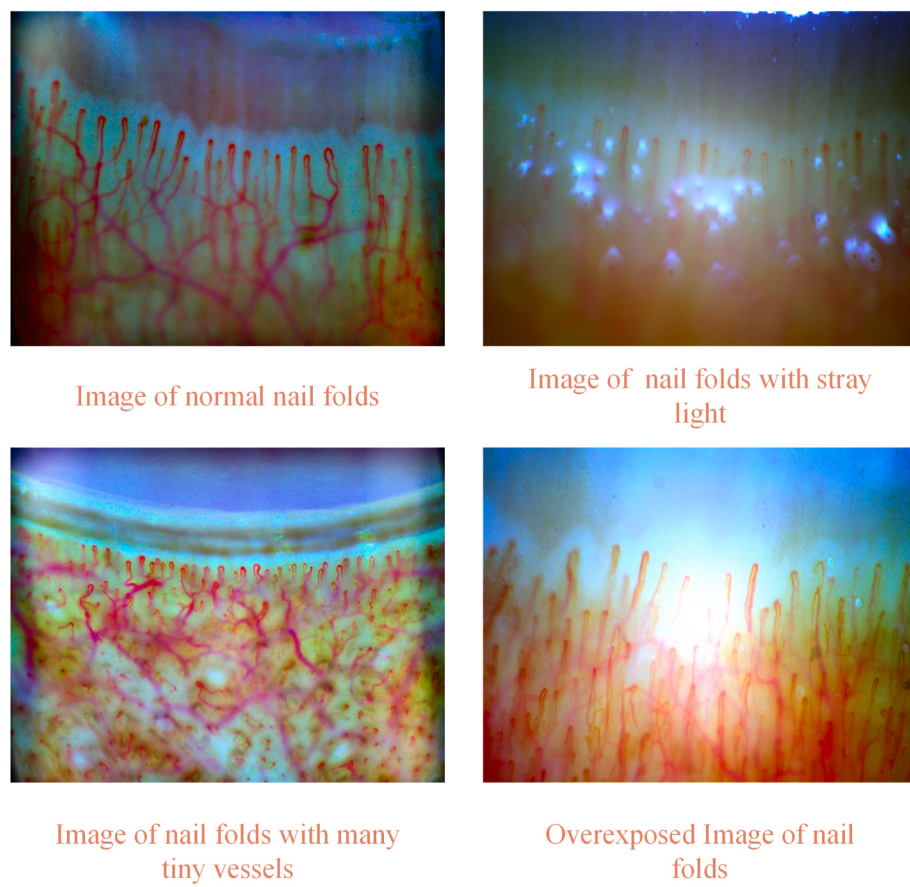


Fig. 9. Four categories of nailfold images.

Table 1
Software and hardware configuration parameters.

Configuration	Parameter
Operation system	Linux
CPU	Intel® Xeon® Platinum 8350C CPU @ 2.60 GHz
GPU	NVIDIA® RTX™ 3090 24G
Pytorch	1.12.1
CUDA	11.3.1

model to detect 300 nailfold images (randomly selected from the nailfold dataset described above).

4.4. Data comparison

To verify the performance of the improved algorithm, the proposed method is compared with the original YOLOv5, YOLOv6, and simple-faster-RCNN, three mainstream target algorithms regarding object loss in validation and AP@0.5. The number of epochs for each of the four algorithms was 150.

Fig. 10 compares the object losses in the validation and AP@0.5 value curves of the proposed method, the original YOLOv5, YOLOv6, and simple-faster-RCNN. The graph on the right shows that after approximately 50 epochs, the AP@0.5 values of the four algorithms began to converge, that of simple-faster-RCNN remained at around 0.42, the value remained between 0.5 and 0.7 in the original YOLOv5, and that of YOLOv6 fluctuated at 0.7. In contrast, the value of our proposed method remained between 0.7 and 0.8; our method exhibited superior performance. The graph on the left indicates that our proposed method converges to a very low value from the first round, and the convergences of the original YOLOv5, YOLOv6, and simple-faster-RCNN are inferior to

that of our proposed method. This indicates that the backpropagation ability of our method is stronger than that of the other three methods in the training process, and our method can converge to the lowest value at the fastest speed.

Table 2 presents the results of our method and those of the original YOLOv5, YOLOv6, and simple-faster-RCNN in terms of parameters, weight size, and average detection time. Comparison of the algorithms demonstrates that our proposed method is superior to YOLOv6 and simple-faster-RCNN, while maintaining high precision, and is slightly inferior to the original YOLOv5. Our proposed method has short training time, small memory usage, fast model initialization speed, and short average detection time under the condition of high precision.

4.5. Filter results comparison

To further validate the effectiveness of our improved method and its accuracy of measurement of nailfold capillary density, the results of the distal capillary count measurement (Fig. 11) and the calculation of nailfold capillary density (Table 3) were compared between the proposed method and the original YOLOv5 for normal, with stray light, with many tiny vessels, and with overexposed nailfold images. To verify the speed of our proposed method, we simultaneously compared the average calculation time of various methods, referring to the average time required by the computer from reading the image to the completion of density calculation. In addition, because there is no quantitative standard for nailfold capillary density, three professionals in nailfold research were recruited to manually examine nailfold images and provide manual measurements as the standard for assessment. For the experts, the average calculation time for an image referred to the average time from the expert's initial image examination to the completion of density calculation.

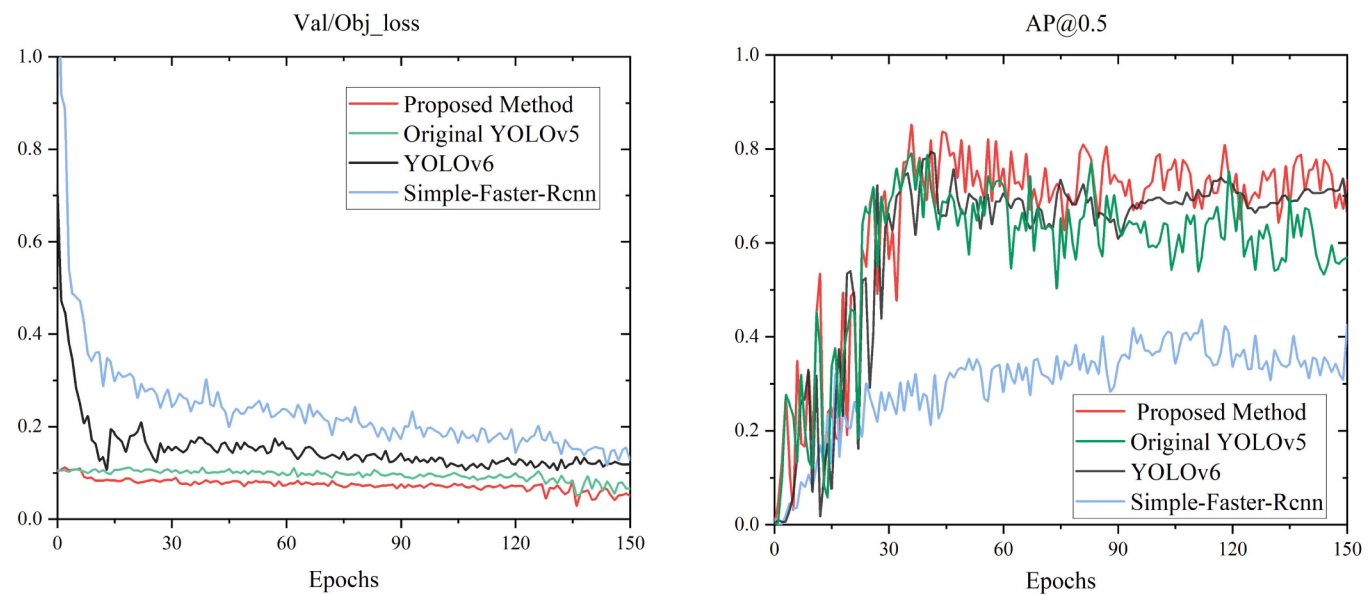


Fig. 10. Loss and AP@0.5 curves.

Table 2
Comparative experimental test results of different networks.

Method	Parameters	Weight size (MB)	Average detection time (ms)
Proposed method	48,804,022	88.5	61.42
Original YOLOv5	46,108,278	88.5	60.35
YOLOv6	76,844,339	154.6	63.31
Simple-faster-RCNN	3,410,982,954	522	2404.47

This experiment used three batches, and each batch selected a typical image from the four image categories as an experimental sample. Three methods (our proposed method, original YOLOv5, and manual calculation by experts) were then used to calculate the densities and compare results. Except for the different experimental samples, the other settings of the three batches were the same. Due to space limitations, only the results of the first batch, Batch 1, are detailed in Table 3, and those of Batches 2 and 3 are elaborated in the appendix.

As shown in Fig. 11, the proposed method was used to screen all distal capillaries in the normal, with stray light, with many small vessels, and with overexposed nailfold images. Whether the vessels were obscured by stray light, densely populated, or amidst overexposure, the proposed method detected and filtered out the distal vessels more effectively than the original YOLOv5.

Density calculations based on the number of distal capillaries were performed, and the results are presented in Table 3. The calculated results of the proposed method were consistent with those calculated by nailfold specialists. Moreover, the average calculation time of our proposed method was 0.064 s, far less than the experts' calculation time. This suggests that our proposed method is faster and can replace manual calculation while maintaining accuracy.

To more intuitively demonstrate the detection performance of our proposed method and the effectiveness of the improved method, Table 4 presents an overall statistical summary using the data from the above experiments. Considering the workload of nailfold experts, the number of pictures in each category is set to 10, which is the size of n in the figure (there are only nine nailfold images with stray light).

5. Conclusions

Nailfold capillary density is an essential physiological parameter for

nailfold health, and many diseases can cause changes in the capillary density. However, in many cases, nailfold images are captured clinically, and many nailfold specialists analyze nailfold images subjectively. Hence, this study proposes an automatic measurement method for nailfold capillary density based on the improved YOLOv5 algorithm and verifies it using the nailfold capillary dataset.

The results show that for the AP@0.5 value, our proposed method improved by 4.92 %, 5.24 %, and 107 % compared with the original YOLOv5, YOLOv6, and Simple-Faster R-CNN, respectively. In addition, the object loss of validation of the proposed method was the smallest. Moreover, in the case of high precision, our method has short training time, small memory usage, fast model initialization speed, and short average detection time. The average detection time for an image is only 0.06 s. Furthermore, for detecting nailfold images in different situations, the proposed method was used to screen distal vessels in normal, with stray light, with many tiny vessels, and with overexposure, and the results were consistent with the manual results by nailfold professionals. Moreover, the calculated densities were consistent with those calculated by nailfold professionals.

Of course, there are some limitations in this research. Because all deep learning algorithms are based on large amounts of data, many resources are required to find and label datasets, and the dataset used in this article is no exception.

In conclusion, the method proposed in this study is robust and suitable for the clinical measurement of nailfold capillary density. In the future, the algorithm performance and detection speed will be further improved concerning network parameters. Research in this field would benefit from adding data from patients with known capillary malformations and assessing the capability of the method to differentiate normal from abnormal vessels.

Funding sources

This work was supported by the Guangdong Provincial Key Field R&D Plan Project (NO. 2020B111120004), the National Natural Science Foundation of China under Grant No. 62075042, the Science and Technology Program of Guangdong Province under Grant No. X190311UZ190, and the 2022 Academic Fund of Foshan University.

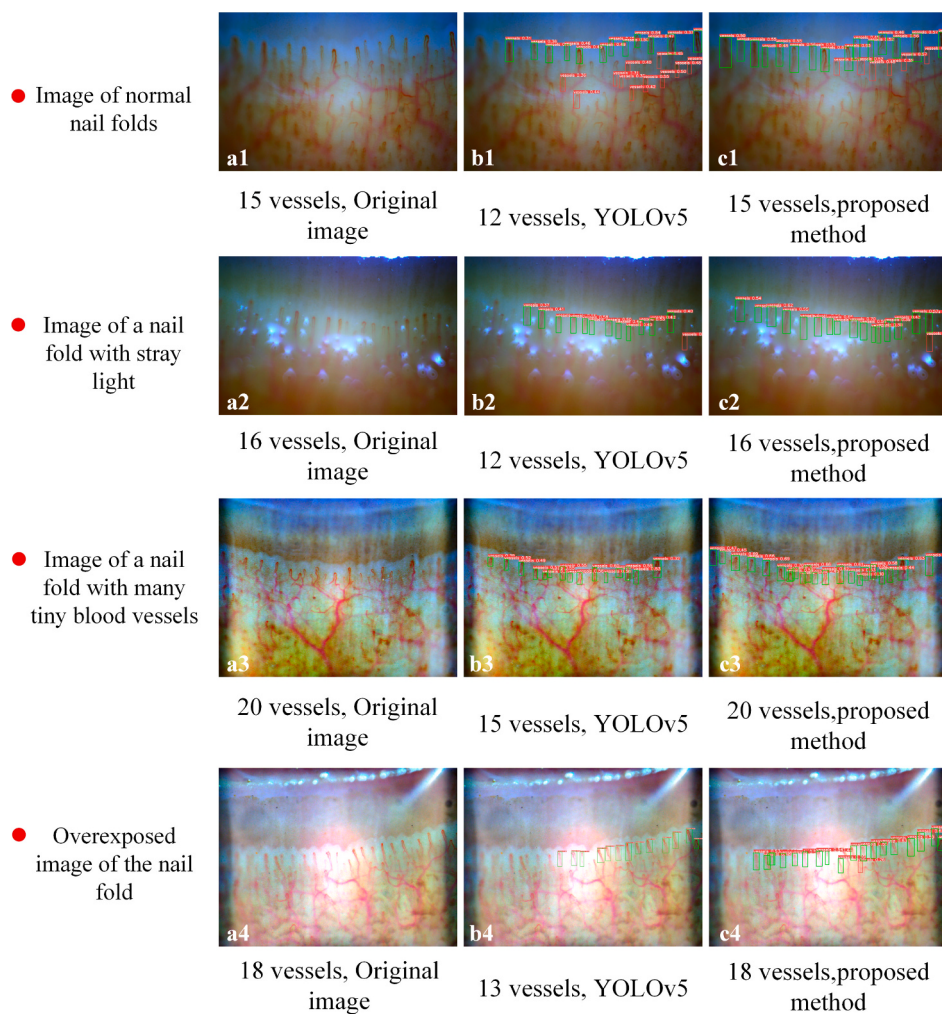


Fig. 11. Distal capillary count—the first batch. The number of vessels in a1–a4 is the number of vessels manually measured by nailfold professionals.

Table 3
Nailfold capillary density^a and calculation time—the first batch.

Method	Normal	With stray light	With many tiny vessels	Over-exposed	Average calculation time (s) ^b
Manual measurement	6.27	6.69	6.31	7.50	61.8
YOLOv5	5.01	5.01	4.30	5.47	0.063
Proposed method	6.27	6.69	6.31	7.50	0.064

^a Measured in units/mm.

^b The average time from reading the image to the completion of density calculation.

Table 4

Matching times^a between experimental method calculation results and expert calculation results.

Method	Normal (n = 10)	With stray light (n = 9)	With many tiny vessels (n = 10)	Over-exposed (n = 10)
YOLOv5	10	8	9	9
Proposed method	3	0	3	2

^a Number of times the results calculated using the experimental method coincides with those manually calculated by experts.

Declaration of competing interest

The authors declare no conflicts of interest related to this study.

Data availability

Data will be made available on request.

Acknowledgments

We thank the thirty volunteers and three nailfold experts for their contributions to this article.

Appendix A. Supplementary data

Supplementary data to this article can be found online at <https://doi.org/10.1016/j.mvr.2023.104593>.

[org/10.1016/j.mvr.2023.104593](https://doi.org/10.1016/j.mvr.2023.104593).

References

- Asad, M.H., Khaliq, S., Yousaf, M.H., Ullah, M.O., Ahmad, A., Chen, Q., 2022. Pothole detection using deep learning: a real-time and AI-on-the-edge perspective. *Adv. Civ. Eng.* 2022, 1–13. <https://doi.org/10.1155/2022/9221211>.
- Cao, M., Fu, H., Zhu, J., Cai, C., 2022. Lightweight tea bud recognition network integrating GhostNet and YOLOv5. *Math. Biosci. Eng.* 19 (12), 12897–12914. <https://doi.org/10.3934/mbe.2022602>.
- El Miedany, Y., Ismail, S., Wadie, M., Hassan, M., 2022. Nailfold capillaroscopy: tips and challenges. *Clin. Rheumatol.* 41 (12), 3629–3640. <https://doi.org/10.1007/s10067-022-06354-1>.
- Emrani, Z., Karbalaei, A., Fatemi, A., Etehad tavakol, M., Erlandsson, B.E., 2017. Capillary density: an important parameter in nailfold capillaroscopy. *Microvasc. Res.* 109, 7–18. <https://doi.org/10.1016/j.mvr.2016.09.001>.
- Girshick, R., Farst, R.-C.N.N., 2015. IEEE International Conference on Computer Vision (ICCV), 2015, pp. 1440–1448. <https://doi.org/10.48550/arXiv.1504.08083>.
- Gracia Tello, B., Ramos Ibañez, E., Fanlo Mateo, P., Sáez Córmet, L., Martínez Robles, E., Ríos Blanco, J.J., Marí Alfonso, B., Espinosa Garriga, G., Todolí Parra, J., Ortego Centeno, N., Callejas Rubio, J.L., Freire Dapena, M., Marín Ballvé, A., Selva-O'Callaghan, A., Guillén Del Castillo, A., Simeón Aznar, C.P., Fonollosa Pla, V., 2022. The challenge of comprehensive nailfold videocapillaroscopy practice: a further contribution. *Clin. Exp. Rheumatol.* 40 (10), 1926–1932. <https://doi.org/10.55563/clinxprheumatol/gusce8>.
- He, K., Zhang, X., Ren, S., Sun, J., 2015. Spatial pyramid pooling in deep convolutional networks for visual recognition. *IEEE Trans. Pattern Anal. Mach. Intell.* 37 (9), 1904–1916. <https://doi.org/10.1109/TPAMI.2015.2389824>.
- Hofstee, H.M., Serné, E.H., Roberts, C., Hesselstrand, R., Scheja, A., Moore, T.L., Wildt, M., Manning, J.B., Vonk Noordegraaf, A., Voskuyl, A.E., Herrick, A.L., 2012. A multicentre study on the reliability of qualitative and quantitative nail-fold videocapillaroscopy assessment. *Rheumatol. (Oxf. Engl.)* 51 (4), 749–755. <https://doi.org/10.1093/rheumatology/ker403>.
- Karbalaei, A., Abtahi, F., Fatemi, A., Etehad tavakol, M., Emrani, Z., Erlandsson, B.E., 2017. Elliptical broken line method for calculating capillary density in nailfold capillaroscopy: proposal and evaluation. *Microvasc. Res.* 113, 1–8. <https://doi.org/10.1016/j.mvr.2017.04.002>.
- Lambova, S., Hermann, W., Müller-Ladner, U., 2011. Capillaroscopic pattern at the toes of systemic sclerosis patients: does it "tell" more than those of fingers? *J. Clin. Rheumatol.* 17 (6), 311–314. <https://doi.org/10.1097/RHU.0b013e31822be4e8>.
- Lawal, M.O., 2021. Tomato detection based on modified YOLOv3 framework. *Sci. Rep.* 11 (1), 1447. <https://doi.org/10.1038/s41598-021-81216-5>.
- Maldonado, G., Chacko, A., Lichtenberg, R., Ionescu, M., Rios, C., 2022. Nailfold capillaroscopy in diabetes mellitus: a case of neo-angiogenesis after achieving normoglycemia. *Oxf. Med. Case Reports.* 2022 (9), omac088. <https://doi.org/10.1093/omcr/omac088>.
- Neubauer-Geryk, J., Hoffmann, M., Wielicka, M., Piec, K., Kozera, G., Brzeziński, M., Bieniaszewski, L., 2019. Current methods for the assessment of skin microcirculation: part 1. *Postepy Dermatol. Alergol.* 36 (3), 247–254. <https://doi.org/10.5114/ada.2019.83656>.
- Ong, Y.Y., Nikoloutsopoulos, T., Bond, C.P., Smith, M.D., Ahern, M.J., Roberts-Thomson, P.J., 1998. Decreased nailfold capillary density in limited scleroderma with pulmonary hypertension. *Asian Pac. J. Allergy Immunol.* 16 (2–3), 81–86.
- Redmon, J., Farhadi, A., 2017. YOLO9000: Better, Faster, stronger IEEE Conference on Computer Vision and Pattern Recognition (CVPR), 2017, pp. 6517–6525. <https://doi.org/10.1109/CVPR.2017.690>.
- Redmon, J., Divvala, S., Girshick, R., Farhadi, A., 2016. You Only Look Once: Unified, Real-time Object Detection IEEE Conference on Computer Vision and Pattern Recognition (CVPR), 2016, pp. 779–788. <https://doi.org/10.1109/CVPR.2016.91>.
- Ren, S., He, K., Girshick, R., Sun, J., Faster, R.-C.N.N., 2017. Faster R-CNN: towards real-time object detection with region proposal networks. *IEEE Trans. Pattern Anal. Mach. Intell.* 39 (6), 1137–1149. <https://doi.org/10.1109/TPAMI.2016.2577031>.
- Sallalmi, M., Oksala, N., Pettilä, V., Tenhunen, J., 2012. Evaluation of sublingual microcirculatory blood flow in the critically ill. *Acta Anaesthesiol. Scand.* 56 (3), 298–306. <https://doi.org/10.1111/j.1399-6576.2011.02569.x>.
- Silva, I., Almeida, C., Teixeira, A., Oliveira, J., Vasconcelos, C., 2016. Impaired angiogenesis as a feature of digital ulcers in systemic sclerosis. *Clin. Rheumatol.* 35 (7), 1743–1751. <https://doi.org/10.1007/s10067-016-3219-8>.
- Tian, J., Xie, Y., Li, M., Oatts, J., Han, Y., Yang, Y., Shi, Y., Sun, Y., Sang, J., Cao, K., Xin, C., Siloka, L., Wang, H., Wang, N., 2020. The relationship between nailfold microcirculation and retinal microcirculation in healthy subjects. *Front. Physiol.* 11, 880. <https://doi.org/10.3389/fphys.2020.00880>.
- Tian, Z.W., Huang, J., Yang, Y., Nie, W.Y., 2023. KCFS-YOLOv5: a high-precision detection method for object detection in aerial remote sensing images. *Appl. Sci. Basel* 13 (1), 649. <https://doi.org/10.3390/app13010649>.
- Zhang, Y.F., Ren, W., Zhang, Z., Jia, Z., Wang, L., Tan, T., 2022. Focal and efficient IOU loss for accurate bounding box regression. *Neurocomputing* 506, 146–157. <https://doi.org/10.1016/j.neucom.2022.07.042>.